Research Paper

Temporal Coordination of Hippocampal Neurons Reflects Cognitive Outcome Post-febrile Status Epilepticus☆,☆☆

Jeremy M. Barry [a],*, Sophie Sakkaki [a], Sylvain J. Barriere [a], Katelin P. Patterson [b], Pierre Pascal Lenck-Santini [c], Rod C. Scott [a,d], Tallie Z. Baram [b], Gregory L. Holmes [a]

[a] Department of Neurological Sciences, University of Vermont College of Medicine, Burlington, Vermont, United States
[b] Departments of Anatomy/Neurobiology and Pediatrics, University of California—Irvine, Irvine, California, United States
[c] Mediterranean Institute of Neurobiology (INMED), U901, INSERM, Marseille, France
[d] Department of Neurology, University College London, Institute of Child Health, United Kingdom

ARTICLE INFO

ABSTRACT

The coordination of dynamic neural activity within and between neural networks is believed to underlie normal cognitive processes. Conversely, cognitive deficits that occur following neurological insults may result from network discoordination. We hypothesized that cognitive outcome following febrile status epilepticus (FSE) depends on network efficacy within and between fields CA1 and CA3 to dynamically organize cell activity by theta phase. Control and FSE rats were trained to forage or perform an active avoidance spatial task. FSE rats were sorted by those that were able to reach task criterion (FSE-L) and those that could not (FSE-NL). FSE-NL CA1 place cells did not exhibit phase preference in either context and exhibited poor cross-theta interaction between CA1 and CA3. FSE-L and control CA1 place cells exhibited phase preference at peak theta that shifted during active avoidance to the same static phase preference observed in CA3. Temporal coordination of neuronal activity by theta phase may therefore explain variability in cognitive outcome following neurological insults in early development.

© 2016 The Authors. Published by Elsevier B.V. This is an open access article under the CC BY-NC-ND license (http://creativecommons.org/licenses/by-nc-nd/4.0/).

1. Introduction

The physiological capacity to coordinate dynamic neural activity within and between neural networks is believed to underlie normal cognitive processes (Fenton, 2015). This theory is largely based upon studies that have observed that the temporal coordination of neuronal firing, with respect to theta oscillations within the hippocampal circuit (Mizuseki et al., 2009), is correlated with learning and memory (Robbe and Buzsaki, 2009; Schomburg et al., 2014; Douchamps et al., 2013; Siegle and Wilson, 2014). Specifically, both modeling and experimental work suggest that the dynamic phase relationships of synaptic

current as well as the timing of action potentials during theta rhythm are critical in both encoding and retrieval by organizing the transfer of neural information between the hippocampus and neocortex and within the hippocampal circuit (Hasselmo, 2005; Siegle and Wilson, 2014). Whether neuronal discoordination has a role in cognitive impairment following neurological insults requires demonstrating a link between temporal discoordination within and between components of the hippocampal circuit and cognitive outcome. If neural coordination by theta oscillations is necessary for cognitive processes, we hypothesized that levels of temporal coordination should reflect cognitive outcome in pathologies where learning and memory deficits are known to occur.

We chose to study febrile status epilepticus (FSE) to test this theory as it is the most common cause of seizures lasting 30 min or more in children (Kravljanac et al., 2015), and increases risk for developing cognitive impairment in both pediatric patients (Martinos et al., 2012; Roy et al., 2011; van Esch et al., 1996) and in the animal model (Dube et al., 2009; Barry et al., 2015). While animal models of febrile seizures are not found to be associated with hippocampal cell loss (Toth et al., 1998; Bender et al., 2003; Dube et al., 2004), febrile seizures have been found to persistently modify inhibitory h-channels (Chen et al., 2001) and alter GABAergic inhibition (Chen et al., 1999). Prolonged febrile seizures, in particular, have been shown to lead to long-term increases in network hyperexcitability (Dube et al., 2000). However, it remains to

be shown that these network changes affect the temporal coordination of action potentials in a manner that could explain cognitive impairment following FSE. To this end we induced prolonged experimental febrile seizures lasting 30 min and investigated seizure-induced changes in temporal coordination through an in vivo study of hippocampal LFPs and CA1 and CA3 place cells. We aimed to evaluate the baseline levels of place cell organization in each region by local theta oscillations for FSE animals that could effectively learn (FSE-L), or were unable to learn (FSE-NL), while simply foraging for food pellets as well as during the active avoidance task.

FSE-NL CA1 place cells did not exhibit phase preference in either foraging or active avoidance contexts and exhibited poor cross-theta interaction between CA1 and CA3. In contrast, FSE-L and control CA1 place cells exhibited a baseline phase preference at peak theta during foraging. However, during performance of the active avoidance task, which necessitated the recall of the shock zone location, the preferred theta phase shifted to the descending phase of theta, matching the static phase preference observed in CA3. Altogether, these results show that dynamic temporal organization of neurons within local theta oscillations, as well as circuit efficacy in local hippocampal networks, reflect cognitive outcome observed post FSE. The results thereby support the notion that neural coordination by local theta oscillations, as well as dynamic theta phase modulation with regard to different aspects of learning and memory, plays an important role in the underpinning of normal cognitive processing as well as cognitive deficits associated with a pediatric seizure model (Hasselmo, 2005; Fenton, 2015).

2. Methods

2.1. Overview

On postnatal day 10 (P10) 7 male Sprague–Dawley rats experienced experimental FSE and 6 littermate rats were removed from the cage and used as controls (Cont). At age 2 months, these animals underwent the training phase for a hippocampal dependent spatial task, the dual reference frame active avoidance task. As described in our previous work, the FSE rats separated into those that met criterion of 5 or fewer consecutive shocks in 2 consecutive sessions (learners [FSE-L]) and those that did not reach criterion by the 15th training session (non-learners [FSE-NL]) (Barry et al., 2015). After acquisition of the active avoidance task, the animals were placed on a food deprivation schedule and exposed to the stable arena for 20 min a day for 5 days while food pellets fell from an overhead feeder every 30 sec. After this period, the animals were trained to alternate from foraging to avoidance contexts in the same arena. At age 3 months, rats were implanted with an array of

micro-electrodes in each hippocampus that allowed for the recording of LFPs and hippocampal place cells in the open field and during the active avoidance task. The recording sessions during the foraging task allowed for the assessment of the temporal organization of hippocampal place cells with uniform spatial sampling in the absence of cognitive demand. In contrast, the recording sessions during the active avoidance task allowed for this assessment in a context with cognitive demand that had separated the FSE animals into learners (FSE-L) and non-learners (FSE-NL). Fig. 1 illustrates the experimental protocol and associated analyses used in our study.

2.2. Induction of Experimental FSE

All procedures were approved by the University of Vermont and UC–Irvine animal care and use committee and conducted in accordance with guidelines from the National Institutes of Health.

Sample size calculation was based on differences between the Cont and the FSE in phase preference of CA1 neurons during active avoidance. Using estimates of standard deviation from our preliminary data of phase preference, a sample size of 80 cells in the Cont and 30 cells in the FSE-L and FSE-NL has 90% power to detect a difference of 30° between means with a significance level (alpha) of 0.05 (two-tailed). We therefore used 13 male Sprague–Dawley rats for the study. The animals were born and maintained in quiet facilities under controlled temperatures and light dark cycle. Their birth was timed within 12 h and the date of birth was considered postnatal day (P) 0.

Experimental FSE was induced for 7 rats as previously described (Dube et al., 2006). On P10, pups were placed in a glass container and their core temperature increased to approximately 40.5 °C using a regulated stream of warm air as a simulation of high fever. Core temperatures were measured at baseline, at seizure onset, and every 2 min during hyperthermia. Hyperthermic seizure onset is heralded by sudden freezing, followed by oral automatisms and forelimb clonus. Seizures progressed to body flexion and one or more tonic stage 5 seizures. In order to more accurately model prolonged FSE in humans that typically last longer than 30 min, hyperthermia (Maximum temperature: 41.5–42.9 °C) was maintained for 34–38 min, resulting in behavioral seizures lasting an average of 36.8 min ($\pm$ 0.24 SEM) (Dube et al., 2010). The Cont group included 6 littermates of the experimental group that were removed from the cage for the same duration to control for potential stress and their core temperatures kept within normal range for age. None of the features associated with hyperthermic induction of FSE at P10 (seizure duration, seizure threshold, maximal temperature or hyperthermia duration) were found to influence the categorization of FSE animals as learners or non-learners (Sup
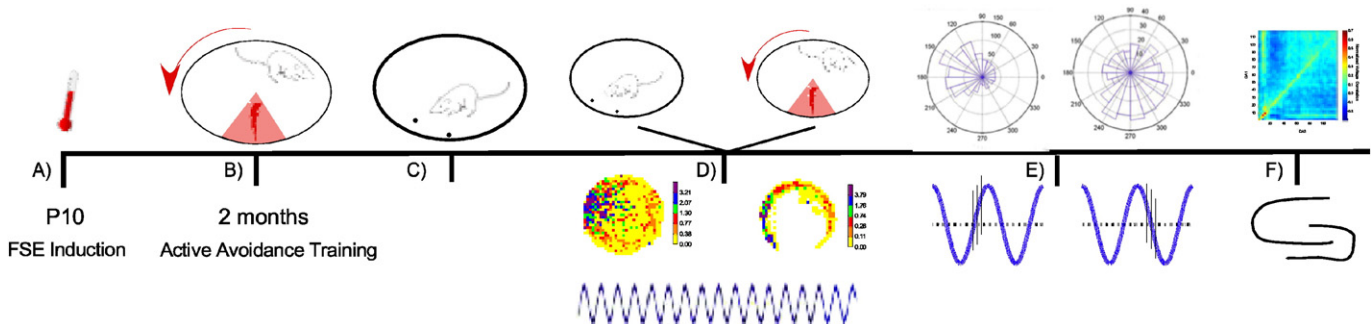

Fig. 1. Illustration of experimental design and analyses. A) On P10 7 rats experienced FSE and 6 rats were used as normothermic Cont (underwent separation from the dam for a matched time period). B) At age 2 months, all rats were trained to perform an active avoidance task in which they learned a hippocampal dependent spatial task which involved the avoidance of a shock zone on a rotating arena. Task measurements were made during this task acquisition phase and FSE animals that failed to meet criterion were designated as FSE-NL and those that did were designated as FSE-L. C) When the rats were approximately 3 months old they were trained to forage for food pellets on the stable arena. Cont and FSE animals were then implanted with an array of micro-electrodes in each hippocampus that allowed for the recording of LFPs and place cells during pellet chasing behavior. D) Two recording protocols were used in the study. The first protocol examined the long-term stability of place cell firing fields in two foraging sessions that were separated by two hrs. The second protocol examined place cell firing field and LFP properties when alternating between foraging and avoidance sessions. E) The temporal coordination of CA1 and CA3 place cells by local theta was analyzed for both foraging and avoidance sessions. F) Voltage correlations between theta signals in both CA1 and CA3 against all LFP signals (1–120 Hz) in the opposite region were analyzed as a means of measuring communication efficacy between the two structures.

Table 1). Moreover, induction of FSE in the animal model has not been found to cause gross morphological changes or lead to cell loss (Bender et al., 2003; Dube et al., 2004; Toth et al., 1998).

2.3. Active Place Avoidance Behavioral Task

The active place avoidance task (Biosignal; Brooklyn, New York) was developed to measure spatial memory and cognition (Pastalkova et al., 2006). In this task, animals learn to associate an unmarked region of space with a mild shock on a constantly rotating arena. The rats must attend to their ever-changing position in the room frame lest they be rotated into the shock zone. Remembering the spatial location of the shock zone in the stationary room frame requires the hippocampus, and in particular, memory retrieval.

At age 2 months, 6 Cont and 7 FSE rats were lightly anesthetized and implanted with a stainless steel safety clip (Eagle Claw, USA, size 12) in the skin on the back of the neck in order to allow for attachment of a cable with an LED. This tether was then used for automated tracking and delivery of a mild electrical shock. Experimenter was blind as to which group each rat belonged.

The arena consisted of a steel disc 82 cm in diameter and was lighted from both above and below. A white cue card with black diagonal lines was placed on the West wall (1.2 m long and 0.75 m high) and a white cue was placed on the East wall (1.2 m long and 0.75 m high). Two proximal cue cards (45 × 62 cm), one black (Color-Aid 9.5 gray) and one white (Color-Aid 2.5 gray) were placed approximately 20 cm from the periphery of the arena and were 135° apart from center to center.

On day one of training, the animal was connected to the cable and allowed to explore the arena for 10 min. On the second day, a clear Plexiglas barrier was placed around the perimeter of the arena that rotated at a rate of one revolution per min. The rat was again allowed to explore the arena for 10 min. On all subsequent days, rats received a 0.2 mA shock in an unmarked 876 cm² triangular sector of the arena covering a 60° arc on the Southern edge of the arena. This sector was stable with respect to the room cues while the arena rotated. The entrance latency of the shock was 1 ms, the shock duration was 0.5 sec and the inter-shock latency was 2 sec. Training was continued with two 10 min sessions per day until criterion was met. It is possible that the rats could simply run through the shock zone after experiencing a shock and not use a hippocampal spatial strategy. If so, at a rotation rate of 1 rpm, the rats would receive a minimum of 10 shocks. Therefore, criterion was set at 5 or fewer shocks within two consecutive sessions. If criterion was not met by the end of training at session 15, the rat was designated a non-learner. An inability to learn this task was considered to have a potentially pathological basis as animals of the same strain and age were previously found to reach criterion within this number of training sessions (Jenks et al., 2013).

2.4. Foraging Task

Approximately 3 weeks following behavioral training in active avoidance, rats were food deprived within 85% of their baseline body weight and trained to chase sugar pellets on the stable, non-rotating arena. The pellets dropped from an overhead feeder every 30 s and fell to a random location in order to encourage spatial sampling of the arena surface area. Pellet-chasing training continued for approximately 20 min a day for 5 consecutive days.

2.5. Surgery

At age 3 months rats underwent implantation of a bilateral array of recording electrodes. The rats were anesthetized with inhaled isoflurane and placed in a stereotaxic frame. The skull was exposed and four screws inserted, two anterior to the left and right ends of

bregma and two left and right over the cerebellum. Grounding was achieved via the right cerebellar screw.

Rats were chronically implanted with a custom implant (Versadrive; Neuralynx, Montana) that allowed for LFP and single cell recording from a 2 × 2 array of tetrodes in both the left and right hippocampus (−3.8 AP, ±3.8 ML, set at ±10°). All tetrodes were made from 25 μm diameter nichrome wire (A–M systems; Carlsborg, WA). Their tips were placed 2.0 mm below the skull surface. For all implants, each tetrode wire was gold plated before implantation until the impedance was between 80 and 200 kΩ.

All implants were fixed to the skull via the skull screws (FHC Inc.) and Grip Cement (Dentsply Inc.). The wound was sutured and topical antibiotic applied. The interval between surgery and the beginning of electrophysiological recording was 1 week.

2.6. Electrophysiology and Recording Protocols

Rats were tethered to a recording cable while they foraged for sugar pellets or during the active avoidance task. Tetrode signals were pre-amplified X 1 at the headstage and channeled through the tether cable to the signal amplifiers and computer interface. LFPs were subsampled at 3000 Hz and filtered at 1–9000 Hz while single units were sampled at 30.3 KHz and filtered at 300–6000 Hz (Neuralynx, Montana). All signals were referenced against a tetrode wire in the near the corpus callosum. The activity of individual units was separated offline into different clusters based on their waveform properties. Waveform properties were defined in 3-dimensional feature space using custom spike-sorting software (Offline Sorter, Plexon, Dallas, TX). A detailed description of cluster quality analysis is provided in supplementary material. Examples of cell clusters recorded from FSE-NL and associated cluster quality analyses are shown in Sup. Fig. 1.

The rat's location in the arena was sampled at 60 Hz (Biosignal, Brooklyn, USA) using a digital camera that detected a light emitting diode (LED) placed near the animal's head. Position and electrophysiology timestamps were synchronized offline using custom software. During active avoidance sessions, an additional LED was detected that was fixed to the rotating arena. The detection of both the LED on the animal and the LED on the arena allowed for calculation of the rat's speed on the rotating platform.

During screening sessions, animals foraged for food pellets on the arena. Electrodes were advanced until contacting the pyramidal cell layer CA1 of the dorsal hippocampus, as characterized by the observation of units as well as 140–200 Hz ripple activity. Tetrodes were also lowered to CA3 to allow for simultaneous recording in both regions. Following the successful isolation of several cells, a recording session would begin and the rat would forage for pellets for approximately 30 min. The recording sessions in the foraging task were primarily used to assess the firing properties of hippocampal place cells and network oscillations in the open field that allowed for uniform spatial sampling of the arena in the absence of cognitive demand.

Rats were then tested for firing field stability or tested in the active avoidance task.

In tests of long-term firing field stability, the animals were moved to their home cages and returned to the arena 2 h later for another 30 min recording session. Long-term firing field stability measurements were carried out to test for possible group differences in the maintenance of hippocampal map representations in the foraging context (Barry et al., 2012; O'Keefe and Nadel, 1978).

To test for performance in the active avoidance task, rats were connected to the shock tether via a pin on the animal's neck. Two min later the arena would begin to rotate and the recording session in the active avoidance context would last for up to 30 min. Recordings were made in the active avoidance context to test for putative differences in place field quality and local network oscillations during the task that might correlate with cognitive outcome. The

alternation from foraging to avoidance was typically separated by 5–10 min and was repeated each recording day. Tetrodes were moved between recording days to avoid sampling the same cells across more than one session.

2.7. Spatial Tuning of Pyramidal Cells and Phase Analysis

Only units that were determined to be pyramidal cells (Robbins et al., 2013; Fox and Ranck, 1981) were considered for analysis. Firing rate maps (Muller et al., 1987) were used for the spatial analysis of cell activity from one recording session per animal.

For inclusion in phase analysis, the firing fields of cells were required to meet the following criteria:

1) Firing rate: The number of spikes fired by the cell in the firing field divided by dwell-time in the field. Only cells with an average in-field firing rate <9 Hz were include in the data set. This threshold was set to avoid including putative interneurons in the dataset.

2) Firing field coherence: Coherence was calculated as previously described (Barry and Muller, 2011) and estimates the local smoothness of the spatial firing distribution from pixel to pixel. Cells with field coherence values >0.2 were included in the analysis.

3) Field size: The field size of firing fields ranged between a minimum of 9 contiguous pixels and a maximum of 700 pixels (approximately 60% of the arena surface).

Phase preference was analyzed for each spatially tuned cell with respect to local theta oscillations in the pyramidal cell layer, either in CA1 or CA3. Several criteria were imposed on the selection of the LFP that was best representative of the local theta signal. LFPs were only considered if they exhibited 140–200 Hz ripple activity, when the rat was at rest, and the wire had at least one cell that met place cell criteria. The selected LFP was filtered between 4 and 14 Hz using Chebyshev type 2 filters, then the phase was extracted using the Hilbert transform. All the spikes recorded from this tetrode and from neighboring tetrodes were assigned a phase value from the ongoing theta phase from the selected LFP. The trough of the theta cycle was assigned as 0°/360° while the peak of the theta cycle was assigned as 180°. The phase value from CA1 and CA3 is out of phase since we only reference cell activity to local theta.

The mean preferred phase of firing (see section on circular statistics below) was calculated for each cell by averaging (circular mean) the angle value of each spike divided by the total spike count. Cells were considered to have a significant phase preference when the p-value calculated with Ralyeigh's test was ≤0.01. The angle and amount of dispersion (Rbar) were then plotted for each cell in each group for regions CA1 and CA3. Larger Rbar values indicate less dispersion of preferred phase throughout the theta cycle.

Only cells determined to be pyramidal cells that met place field criteria and showed a significant phase preference were included in analysis. Sup. Fig. 3 shows an example of a rate map and place cell firing field (A) as well as extracted phase of local theta (B) and how rate and phase can be combined to create a phase map (Harris et al., 2002) (C). The phase map, averaged over the 30 min recording session, shows that the action potentials of the cell tend to fire throughout the theta cycle as the animal moves through the field. Taken together, the firing rate map and the phase map illustrate that in the field the spikes tend to fire in a phase range between 240° and 320°. This is in good agreement with the rose plot histogram (D), showing the phase distribution of this cell.

Comparisons between phase preference and the phenomenon of phase precession are briefly discussed in supplementary material.

At the group level, the Rayleigh's test was used to determine if the distribution of preferred phase in each group was uniform. The mean preferred direction and strength of theta phase preference was then calculated for the cell population in each group, where the strength of phase modulation was represented as the length of the vector.

2.8. Signal Processing of LFPs

LFP signals were analyzed using the Matlab Signal Processing Toolbox (Mathworks, Inc.) and the Chronux toolbox (Mitra and Bokil, 2008). Spectrograms (1 s window, 1 s overlap, [3,5] tapers, 1–140 Hz) computed from fast Fourier transforms were performed over time course of the recording sessions. Only segments where the animal's speed was equal or greater to 5 cm/sec were included in the analysis. The mean frequency and power (normalized by the sum of the spectrum) of the signal was calculated in theta (5–12 Hz) and slow gamma (25–50 Hz) bands. The relationship between these bands of interest post signal processing and foraging behavior on the stable arena can be seen in Sup. Fig. 2. The justification for studying these frequency bands is discussed in supplementary material. We also analyzed the relationship between animal speed and theta frequency in a similar manner to previous work (Richard et al., 2013).

Although theta rhythms are known to flow as a wave across the longitudinal (septo-temporal) axis (Lubenov and Siapas, 2009) much less is known regarding the organization of theta oscillations between CA1 and CA3 and what long-term effects febrile seizures may have on this organization. We therefore use voltage correlations to examine putative group differences in the functional connectivity between these hippocampal subregions at a wide range of frequency bands during theta-related brain states. Voltage correlations reflect state changes coupled across networks that are driven by neuromodulatory systems (Munk et al., 1996). Studies have shown that voltage correlations can provide a measure of large-scale interactions between cortical areas that are indirectly connected through polysynaptic pathways (de Lange et al., 2008; Mazaheri et al., 2010). Voltage correlations can therefore allow for informative inferences regarding the large-scale oscillatory interactions between brain regions that mediate cognition. If voltage correlations are high, they suggest that there is a greater co-modulation of frequency between two signals. Oscillations that have antithetical patterns will tend to exhibit negative voltage correlations.

Voltage correlations were calculated between signals in the CA1 theta band with ipsilateral CA3 signals between 1 and 120 Hz (resolution of 0.745 Hz) for 3 animals in each group during a single foraging session. This analysis was also done vice versa, comparing CA3 theta with signals between 1 and 120 Hz from ipsilateral CA1. For each recording in each region, the LFP channel with the best theta/delta ratio was selected. The spectrogram was calculated for the first 10 min using the 'cohgramc' function (http://chronux.org) with tapers [3,5], a frequency range of 1–120 Hz and a time window of 1 sec advanced in 1 sec steps. We then computed Pearson's linear correlation coefficient between each electrode pair in each hippocampal field. Finally, a matrix of normalized correlation by frequency was generated for individual animals in each group. These matrices were then exported to SPSS software for statistical analysis. Comparisons against 0 were made for frequency correlations in each group and group by frequency comparisons were also carried out.

2.9. Statistical Analysis

2.9.1. Circular Statistics

In both behavioral and phase analysis (see below) we used circular statistics in order to describe group differences in spatial sampling within a circular arena and preferred phase of cell firing within the filtered theta cycle. This analysis entails the use of Rayleigh's test for non-uniformity of circular data [Rbar = n ∗ r] (Fisher, 1993) where n is the sum of the number of incidences in cases of binned angle data and r is

the resultant vector length of the distribution. The use of the Rayleigh test is described in more detail with regard to behavioral and phase analysis below.

To test the changes in the circular distribution of preferred firing phase between foraging and avoidance contexts, we used the parametric Watson–Williams multi-sample test for equal means, used as a one-way analysis of variance for circular data (Berens, 2009). This analysis was not performed if there was no statistical significance with regard to preferred firing phase in one of the recording contexts.

2.9.2. Behavioral Analysis

Spatial sampling analyses that quantified the rat's movement in the arena during both foraging and avoidance contexts was carried out using Biosignal Tracker software (Biosignal, Brooklyn, USA) for all place cell recording sessions. The surface area of the arena was binned in 10° sections between 0 and 360°. The angle and length of the resultant vectors represent the proportion of time spent at each angle of the arena. Key variables of the behavioral analysis are described below:

A) Dwell time: The arena surface was divided into an array of pixels and the sample time in each pixel was calculated. Dwell-time maps were created where black pixels indicate non-sampled regions and the blue to red color continuum indicates the least to most sampled locations on the arena surface.
B) Rayleigh vector: The length of the resultant vector from the circular analysis is calculated using the formula:
$$r = \sqrt{x^2 + y^2}$$
where x and y are the coordinates of the mean angle and r is the mean vector (Fisher, 1993). The mean and standard error of the Rayleigh vector length in multiple sessions per animal for each group was also calculated.
C) Annular maximum: The proportion of time spent in each of eight equal-area annuli bins on the periphery of the arena was calculated. The annular bin where the greatest proportion of time was spent was considered the annular maximum. Mean and standard error of the annular maximum in multiple sessions per animal for each group was calculated.

2.9.3. Firing Field Stability

Positional firing stability was estimated from the similarity of the place cell's spatial firing pattern between two foraging sessions or between a foraging and avoidance session. Similarity is the Fisher z-transform of the product–moment correlation between the firing rates in corresponding pixels for both intervals. Normalized correlations were used in subsequent analysis (see Section 2.9.4).

In the case of contextual remapping between foraging and avoidance contexts, there were 3 categories of changes with regard to the location of place cell firing fields:

A) Field shift: Cell meets firing field criteria in both foraging and avoidance contexts.
B) Field off: Cell meets firing field criteria in the foraging context but not in the avoidance context.
C) Field on: Cell does not meet firing field criteria in the foraging context but does meet criteria in the avoidance context.

The number of cells in each category was calculated for each group and compared using Chi square analysis.

2.9.4. General Estimating Equations (GEE)

As the behavioral and place cell dataset contains data from multiple sessions in single animals and the LFP dataset contains data from up to 3

recording sessions from each animal, the assumptions of independence of observations are invalid. The observations for each of these measures within single animals are likely to be correlated, and these data can be represented as a cluster. In this case, the existence of a relationship between each measure of interest within an individual animal may then be assumed (Ziegler et al., 1998). In this study we used GEE (SPSS; Armonk, NY), a class of regression marginal model, for exploring multivariable relationships between clustered response data in Cont and FSE animals sorted by cognitive outcome in the active avoidance task. In all GEE analyses, variability between animals is described as standard error of the mean rather than standard deviation. At the behavioral level we tested for differences in the annular maximum. At the single cell level we examined whether the firing field properties, stability, coherence, in-field firing rate and field size, differed between Cont, FSE-L and FSE-NL. At the LFP level we examined whether the mean frequency and mean normalized amplitude at theta and slow gamma frequencies differed between Cont, FSE-L and FSE-NL. We also used GEE to compare
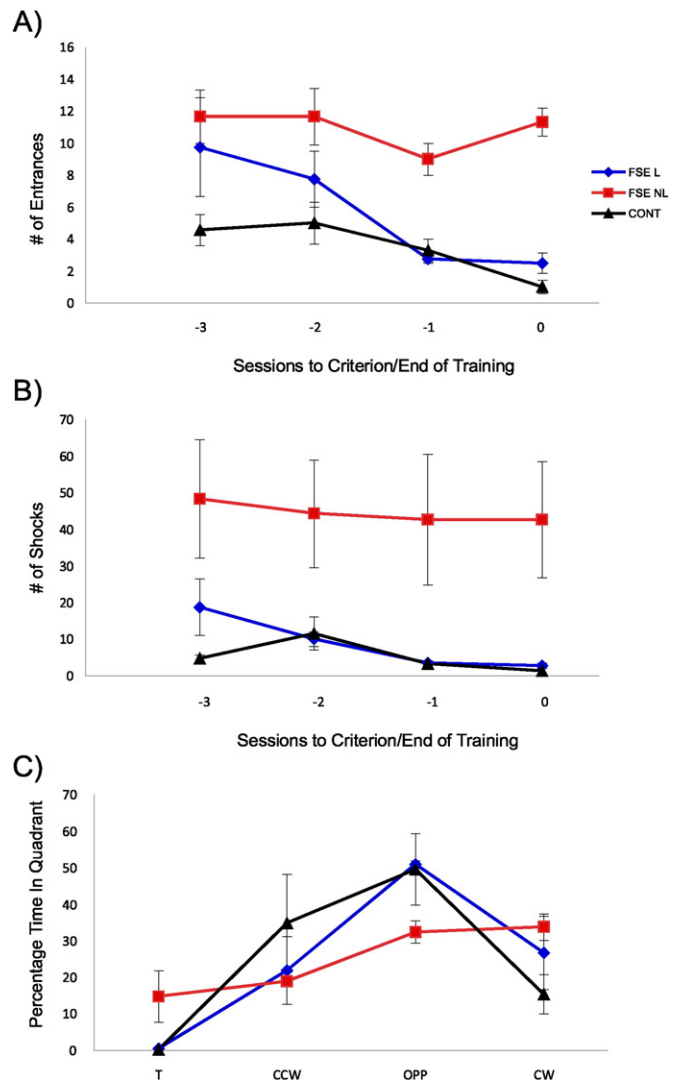

Fig. 2. Mean and standard error of the number of entrances, number of shocks and time spent in each quadrant during each of the final 4 training sessions per animal and group. A) Average number of entrances into the shock for FSE-NL (red line), FSE-L (blue line) and Cont (black line); B) Average number of shocks per group; C) Percentage of time spent in each quadrant in the final training session (FSE-NL) or at criterion (Cont and FSE-L) (T = Target; CCW = quadrant counter-clockwise from shock zone; OPP = quadrant opposite shock zone; CW = quadrant clockwise shock zone).

theta band voltage correlations in CA1 or CA3 with frequencies in the 1–120 Hz range between Cont, FSE-L and FSE-NL. GEE was also used to show when normalized correlations differed from 0 for each individual group for CA1-CA3 comparisons, as well as to examine group by frequency interactions for CA1–CA3 comparisons.

2.10. Histological Procedures

Rats received a lethal dose of isolfurane and were perfused intracardially with saline followed by 4% formaldehyde. The brains were extracted and stored in 4% formaldehyde and
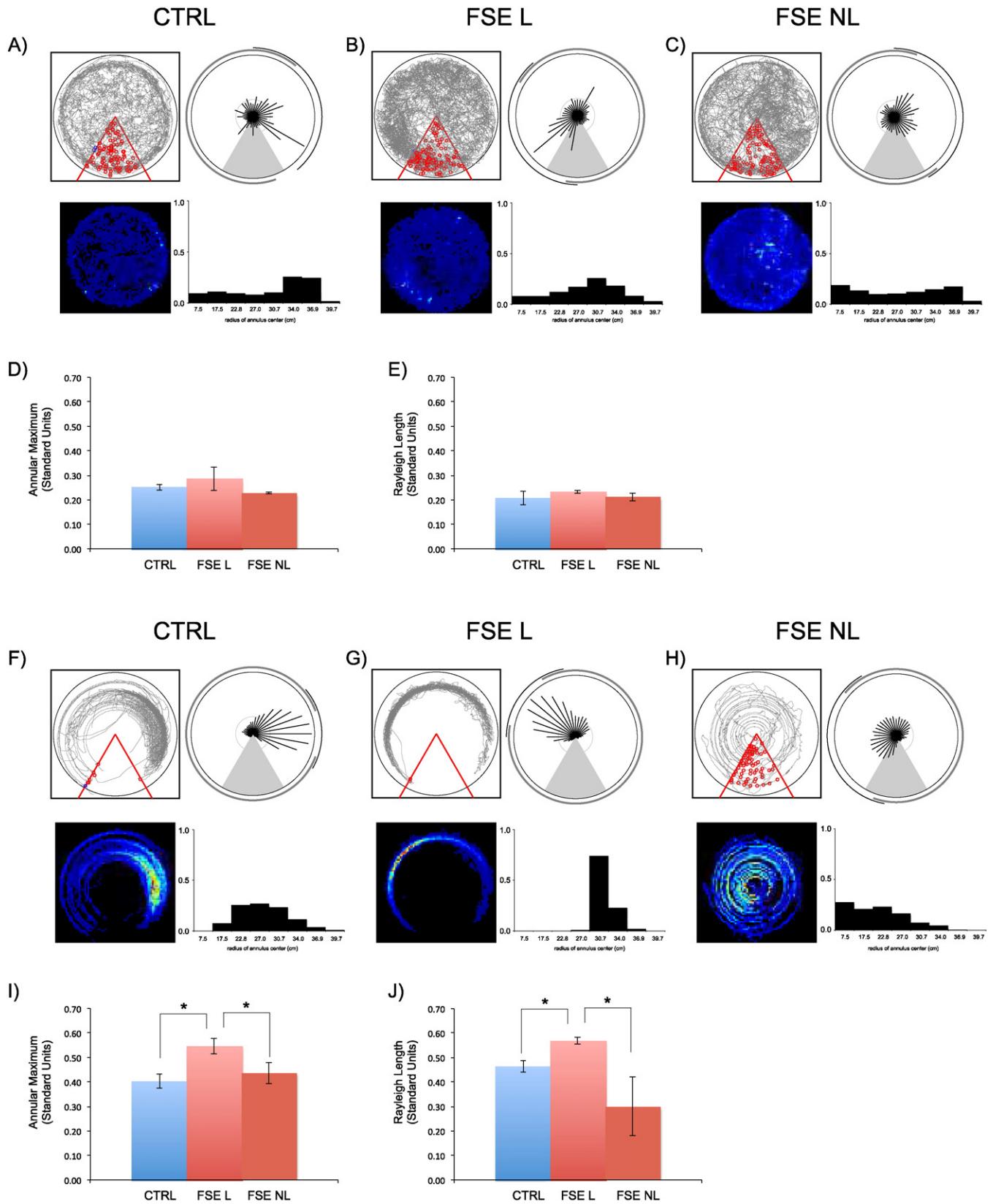
frozen coronal sections (30 μm) were cut and stained with cresyl violet (see example in Sup. Fig. 4). Electrode position was assessed in all rats.

3. Results

3.1. FSE Rats Separate into Learners and Non-learners

The sample of Cont (N = 6) all met task criterion of 5 or fewer shocks in 2 consecutive sessions within 15 training sessions. However, the sample of FSE animals separated into those that met criterion (FSE-L, N = 4) and those that did not (FSE-NL, N = 3).

GEE analysis revealed significant group differences for several key measures of performance in the active avoidance task during the final training trial. Both Cont. and FSE-L showed no difference in performance measures (see Fig. 2) while FSE-NL received significantly more shocks (p < 0.001), made more entrances into the shock zone (p < 0.001), and spent more time in the shock zone (p < 0.001) than Cont. or FSE-L. While cognitive outcome was not influenced by details of FSE induction (Sup Table 1) the results of many of the analyses concerning place cell firing field and LFP properties that follow serve to illustrate several alterations at the cell and network levels in both groups of FSE animals that make them different from Cont.

3.2. Group Differences in Active Avoidance

FSE-NL failed to reach criterion of 5 or fewer shocks in 2 consecutive sessions within 15 training sessions. A description of avoidance behavior in the last 4 sessions of the training phase for each group can be seen in Fig. 2. FSE-NL tend to enter the shock zone more often than Cont and FSE-L (Fig. 2A) and therefore receive more shocks (Fig. 2B). While both Cont and FSE-L tend to spend the majority of their time during the 10 min training session in the area opposite the shock zone (Fig. 2C), FSE-NL animals are less likely to clear the shock zone upon receiving shocks and therefore spend more time in the shock zone. Statistical analysis of these aspects of active avoidance that define cognitive outcome for each group can be found in supplementary material.

During foraging sessions in the recording phase, rats in all groups sample the entire surface of the arena (Fig. 3A-C), and frequently enter the middle of the arena and the shock zone location. Several recording sessions (RS) were sampled per group (Cont, N = 6 and RS = 60; FSE-L, N = 4 and RS = 32; FSE-NL, N = 3 and RS = 37). No significant group effect was found during the foraging context with regard to the annular maximum (Fig. 3D) and mean preferred angle resultant (Fig. 3E).

In the context of avoidance, Cont and FSE learner groups avoided the shock zone and moved in a discrete arc toward the perimeter of the arena (Fig. 3F–G). Conversely, FSE-NL typically received shocks and moved to the center of the arena or ran to the opposite side of the arena (Fig. 3H). These are ineffective avoidance strategies and prevent the rats from reaching criterion of 5 or fewer shocks in 2 consecutive sessions. Several RS were sampled for each rat per group (Cont, N = 6

and RS = 24; FSE-L, N = 4 and RS = 17; FSE-NL, N = 3 and RS = 16). A significant group effect (p = 0.003) was found with regard to the annular maximum (Fig. 3I) between Cont (Mean = 0.40 ± 0.028, FSE-L (Mean = 0.55 ± 0.032), and FSE-NL (Mean = 0.44 ± 0.044). In a complimentary fashion, a significant group effect (p < 0.001) was also found in the mean Rayleigh length (Fig. 3J) between Cont (Mean = 0.46 ± 0.024), FSE-L (Mean = 0.57 ± 0.014), and FSE-NL (Mean = 0.30 ± 0.118). The annular maximum is significantly greater for FSE-L than Cont (p = 0.001) and FSE-NL (p = 0.045), also matched by a significantly greater Rayleigh length in comparison to Cont (p < 0.001) and FSE-NL (p = 0.025). The larger annular maximum indicates that FSE-L spent more time in a singular annular bin and the larger Rayleigh length indicates that the FSE-L moved in a smaller arc during active avoidance. Taken together, these measures evince a more spatially conservative avoidance strategy on the part of FSE-L as they exhibit a reluctance to move over the surface of the arena and tend to stay in a small arc during avoidance.

In comparison of the behavioral analysis between foraging and avoidance contexts, it is apparent that all animals enter the center of the arena and the shock zone location in the foraging context. This demonstrates that, as a feature of the repeated alternation over the course of training and repeated recording sessions, the animals are capable of dissociating the two contexts in the same physical space. Moreover, the fact that FSE-L do not show any significant preference for the periphery of the arena during foraging means that a spatially conservative strategy during active avoidance is not a symptom of general anxiety.

3.3. Place Cell Firing Field Properties are Affected by FSE

Key firing field properties were analyzed for each group including, long-term firing field stability in the foraging context, as well as mean firing field coherence, firing rate and field size for each group during the active avoidance context. These analyses are discussed in more detail in supplementary results. The results indicate that FSE firing fields are less stable over 2-hour periods in comparison to Cont (see Sup. Fig. 5). Replicating our previous work, FSE-NL place cells have a significantly higher firing rate than Cont. and FSE-L (see Sup. Fig. 6) (Barry et al., 2015). The key results are also summarized in Sup. Table 2.

3.4. All Groups Show Contextual Remapping

While the switch between foraging and avoidance contexts occurs in the same physical space (Sup. Fig. 7A), the changes in task demands were sufficient to induce 'remapping' (Muller and Kubie, 1987). The mean firing field correlations for place cells in the foraging context and subsequent exposure to the avoidance context indicates that there was little stability between both contexts for Cont, FSE-L and FSE-NL (r < 0.07). GEE analysis showed that there was no significant group effect (p = 0.092) with regard to firing field correlations between Cont place cells (n = 203, Mean = 0.03 ± 0.006), FSE-L place cells (n =

Fig. 3. Analysis of spatial sampling per single foraging (A–E) and avoidance sessions (F–J) for individual animals. (A–C, F–H). Top Left — Path taken by rat (grey line) over the surface of the stable arena. The red triangle indicates the location of the shock zone in the avoidance context and the epochs where the rat would have received an electric shock are indicated by red circles; Top Right – Polar analysis of spatial sampling where the vector, angle and length of the black lines emanating from the plot center indicate the proportion of time spent at each angle of the arena (0–360° in 10° bins). The outside arc (thin black line) for each plot indicates the distribution of the longest vector lengths that account for at least 50% of the session duration; Bottom Left — Dwell time map (64 pixel resolution) where black pixels indicate non-sampled regions and the blue to red color continuum indicates the least to most sampled locations on the arena surface. Bottom right — Histogram indicating the proportion of time (y-axis) spent in each of eight equal-area annuli bins indicating the radius of the annulus center (x-axis). The annular bin where the greatest proportion of time is spent is considered the annular maximum; D,I) Mean and standard error of the annular maximum in multiple sessions per animal for each group; E,J) Mean and standard error of the length of the resultant Rayleigh vector from all the vectors in the polar plot for multiple sessions per animal for each group. Taken together, the plots indicate that the animals evenly sampled the arena and freely moved through the arena enter and shock zone location during the foraging context. Cont and FSE-L tend to move in a discrete arc while avoiding the shock zone while FSE-NL tend to receive shocks and move to the other side of the shock zone or move to the middle of the arena. FSE-L exhibits a more conservative avoidance strategy by spending more time on the arena annulus and moving in a smaller avoidance arc.

Table 1
Mean standard error of preferred theta phase for CA1 and CA3 place cells during foraging (blue text) and avoidance (red text) recording sessions.

Forage/Avoid	Group	Mean phase	STDERR	Forage/Avoid	Group	Mean phase	STDERR
CA1	CTRL (n = 154)	214.29	0.2180	CA3	CTRL (n = 50)	256.69	0.1878
	FSE L (n = 75)	180.48	0.1317		FSE L (n = 37)	224.60	0.1782
	FSE NL (n = 69)	194.23	0.1893		FSE NL (n = 52)	226.32	0.1429
CA1	CTRL (n = 78)	260.12	0.0182	CA3	CTRL (n = 26)	254.97	0.2563
	FSE L (n = 41)	234.91	0.1727		FSE L (n = 21)	204.55	0.1306
	FSE NL (n =31)	184.49	0.3049		FSE NL (n = 19)	174.18	0.2014

92, Mean = 0.02 ± 0.01) and FSE-NL place cells (n = 128, Mean = 0.01 ± 0.007) (Sup. Fig. 7B).

The number of place cells from each group that were recorded in the foraging context that either shifted their location of firing or no longer meet field criteria in the avoidance context are shown in Sup. Table 3. The number of cells that do not meet field criteria in the foraging context but develop firing fields in the avoidance context are also shown. Analysis of the frequency distribution revealed no significant differences in the occurrence of each remapping type in each group (χ^2 = 8.19, p = 0.085). Examples of place cells of each remapping category between foraging and avoidance contexts are shown in Sup. Fig. 7C–D.

Taken together with the behavioral data in Fig. 3, the lack of firing field similarity between foraging and avoidance indicates that all animals were able to differentiate between both contexts in the same physical space. This data replicates previous work that has shown place cell remapping in the same physical space when rats perform a task (Markus et al., 1995) or experience fear conditioning (Moita et al., 2004).

Moreover, the data indicates that while the FSE-NL were unable to reach criterion with extended training, they were capable of segregating representations of both contexts. Thus, the impaired spatial cognition seen in the FSE-NL was not due to an inability to distinguish two different contexts.

3.5. FSE-NL Lack Temporal Coordination in CA1

The temporal organization of action potentials within the theta cycle has been hypothesized to be a key mechanism by which oscillations influence cognition, learning and memory (Robbe and Buzsaki, 2009; Schomburg et al., 2014; Douchamps et al., 2013; Siegle and Wilson, 2014). Analysis of the preferred firing phase of neurons in CA1 and CA3 was carried out for all place cells that exhibited a significant phase preference within the local theta cycle. No group differences were found with regard to the number of place cells that exhibited

theta phase preference in either cell region or context (see supplementary results). The mean and standard error of the preferred theta phase for CA1 and CA3 place cells during foraging and avoidance contexts are shown in Table 1.
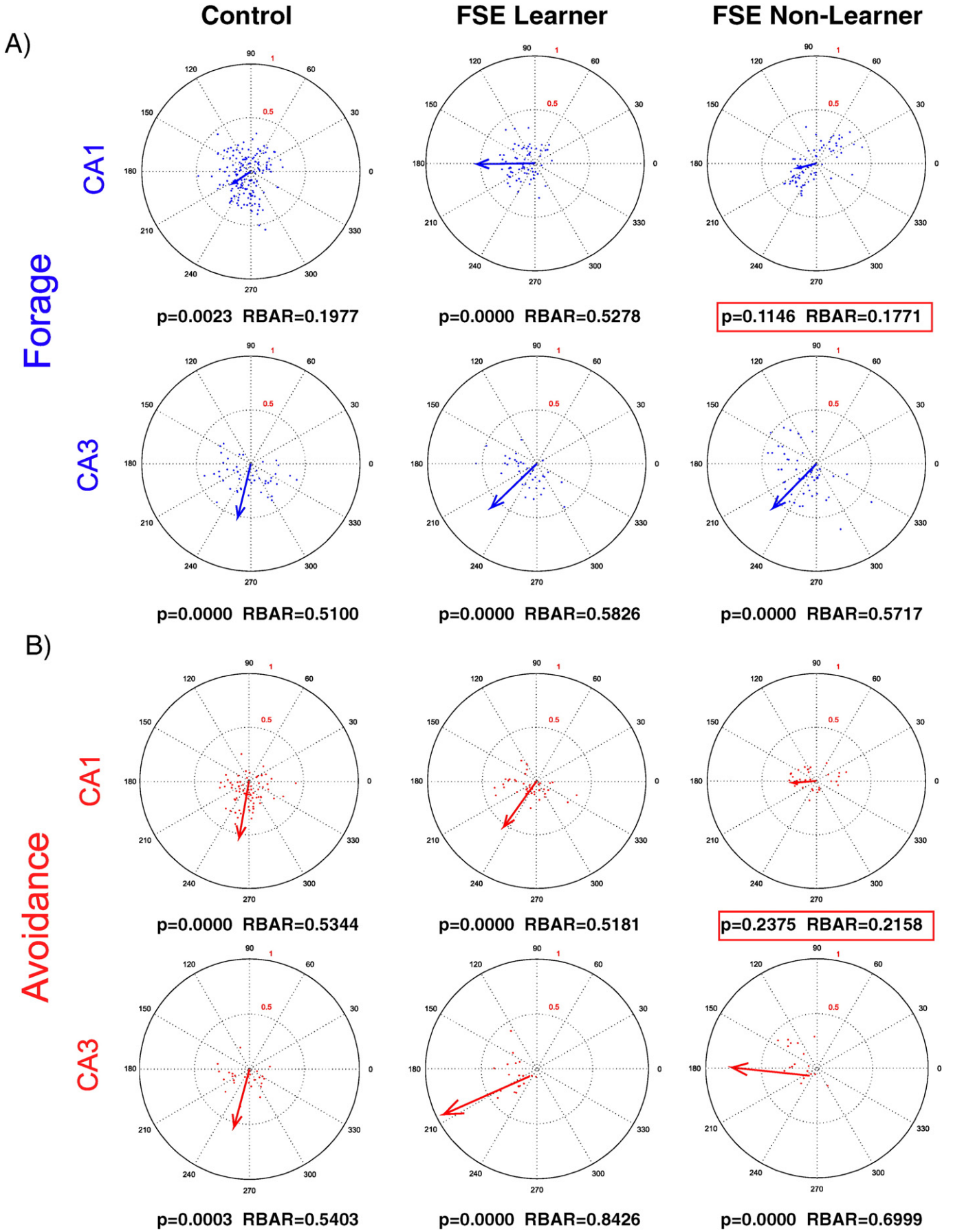
3.5.1. Foraging Context

The preferred firing phase of spatially tuned cells relative to local theta in pyramidal cell layers was analyzed in the foraging task (Fig. 4A) for 6 Cont (N_{CA1} = 154; N_{CA3} = 50), 4 FSE-L (N_{CA1} = 75; N_{CA3} = 37) and 3 FSE-NL (N_{CA1} = 69; N_{CA3} = 52). The phase preference of Cont CA1 place cells was distributed throughout the theta cycle but showed significant phase preference at 214° ± 0.218 (Rbar = 0.198, Rayleigh's test p = 0.0023). The place cells recorded from FSE-L showed a mean phase preference at 180° ± 0.137 (Rbar = 0.53, Rayleigh's test p < 0.0001). Using the Watson–Williams two-sample test (W–W), we found that the mean phase preference for FSE-L cells was more aligned at the peak of theta than Cont (W–W, $F_{(1,227)}$ = 6.54, p = 0.011). In contrast, while place cells recorded from FSE-NL had a mean angle of 194° ± 0.1893, they showed no significant phase preference (Rbar = 0.177, Rayleigh's test p = 0.115).

The lack of significant phase preference for FSE-NL place cells could have been due to phase modulation at opposing angles that could lead to a canceling out of the mean resultant vector length. We therefore analyzed the mean preferred phase of theta per animal (Sup. Table 10). The three animals showed a mean preferred phase for place cell firing that ranged between 132° and 219°. That 2/3 of the animals exhibited dispersion of preferred firing phase across the spectrum suggests that a lack of organization in FSE-NL place cells strongly contributes to the non-significant mean resultant vector length for the group.

The phase preference of CA3 place cells recorded from all groups showed significant phase preference toward the descending phase of local theta in the CA3 pyramidal cell layer. The preferred phase in Cont was 257° ± 0.1878 (Rbar = 0.510, Rayleigh's test p < 0.0001). The place cells recorded from FSE-L showed a mean phase preference at 225° ± 0.1782 (Rbar = 0.583, Rayleigh's test p < 0.0001). While

Fig. 4. Phase analysis of spatially tuned cells relative to local theta in pyramidal cell layers CA1 and CA3 during foraging and avoidance sessions. A) Distribution of preferred firing phases for place cells recorded during foraging sessions in CA1 from Cont (left), FSE-L (middle), FSE-NL (right). Cells recorded from Cont were distributed throughout the theta cycle but showed a significant phase preference at 214°. Cells recorded from FSE-L were more likely to show phase preference at the peak of local theta at 180° than animals from the other 2 groups. While place cells recorded from FSE-NL had a mean angle of 194°, they showed no significant phase preference. The distribution of preferred firing phases for cells recorded in CA3 from Cont (257°, bottom left), FSE-L (225°, bottom middle), FSE-NL (226°, bottom right) all exhibited significant phase preference. No significant differences were found in the distribution of phase preference between the 3 groups. B) Distribution of preferred firing phases for place cells recorded during avoidance sessions in CA1 from Cont (left), FSE-L (middle), FSE-NL (right). Cells recorded from Cont significantly shifted phase preference to the descending phase of theta at 260°. Cells recorded from FSE-L also shifted phase toward the descending phase of local theta and exhibited a preferred firing phase at 234°. Again, FSE-NL displayed a lack of significant phase preference with respect to local theta but had a mean phase preference at 184°. Significantly more place cells displayed a phase preference between 180 and 270° in Cont and FSE-L than FSE-NL. As in the foraging context, the distribution of preferred firing phase for cells recorded in CA3 from Cont (255°, Bottom Left), FSE-L (205°, bottom middle), FSE-NL (174°, bottom right) showed significant phase preference. No significant differences were found in the distribution of phase preference between the 3 groups in CA3 during avoidance. Taken together, the preferred firing phases in CA3 are significant for all 3 groups and remain relatively constant in both contexts. The shift away from a preferred firing phase at the peak of local theta to the descending phase seen in both Cont and FSE-L would put active cells in each cell layer in similar alignments with regard to local theta and may indicate network alterations to adjust for increased cognitive demand. That cells recorded from FSE-L should exhibit significant phase preference both with and without cognitive demand is indicative of network adaptations in these animals that may improve the likelihood of learning the active avoidance task. That CA1 cells recorded from FSE-NL did not show significant phase preference and did not shift to the descending phase of theta during active avoidance is indicative of network malfunction.

Control **FSE Learner** **FSE Non-Learner**

A)

Forage

CA1

p=0.0023 RBAR=0.1977 p=0.0000 RBAR=0.5278 p=0.1146 RBAR=0.1771

CA3

p=0.0000 RBAR=0.5100 p=0.0000 RBAR=0.5826 p=0.0000 RBAR=0.5717

B)

Avoidance

CA1

p=0.0000 RBAR=0.5344 p=0.0000 RBAR=0.5181 p=0.2375 RBAR=0.2158

CA3

p=0.0003 RBAR=0.5403 p=0.0000 RBAR=0.8426 p=0.0000 RBAR=0.6999

place cells recorded from FSE-NL had no significant phase preference in CA1, place cells in CA3 had a significant phase preference at 226° ± 0.1429 (Rbar = 0.572, Rayleigh's test p < 0.0001). As all groups demonstrate a preferred phase of firing in CA3, this implies that network alterations in relation to cognitive outcome are specific to CA1.

3.5.2. Avoidance Context

Following the recording sessions in the foraging context, the same animals were recorded in the avoidance context. Phase analysis revealed the preferred firing phase of place cells relative to local theta in pyramidal cell layers of CA1 and CA3 during the active avoidance task (Fig. 4B) for Cont (N_{CA1} = 78; N_{CA3} = 26), FSE-L (N_{CA1} = 41; N_{CA3} = 21) and FSE-NL (N_{CA1} = 31; N_{CA3} = 19). The phase preference of CA1 place cells recorded from Cont showed significant phase preference at 260° ± 0.0182 (Rbar = 0.534, Rayleigh's test p < 0.0001). Similarly, the place cells from FSE-L showed a significant phase preference at 235° ± 0.1727 (Rbar = 0.518, Rayleigh's test p < 0.0001). While place cells from FSE-NL had a mean angle of 185° ± 0.3049, they again showed no significant phase preference (Rbar = 0.216, Rayleigh's test p = 0.238).

The phase preference of CA3 place cells recorded from Cont and FSE-L again showed a significant phase preference toward the descending phase of theta. The preferred phase in Cont was 255° ± 0.2563 (Rbar = 0.540, Rayleigh's test p = 0.0003). The place cells recorded from FSE-L had a mean phase preference at 205° ± 0.1306 (Rbar = 0.843, Rayleigh's test p < 0.0001). As in the foraging context, CA3 place cells recorded from FSE-NL again showed a significant phase preference, although at 174° ± 0.2014 (Rbar = 0.700, Rayleigh's test p < 0.0001).

3.5.3. CA1 and CA3 Phase Preferences Align During Task Performance

We directly compared the preferred phase of place cell activity in the baseline foraging session with the subsequent avoidance session on the same day of recording, separated by approximately 5–10 min. Preferred firing phase for CA1 place cells in Cont shifted significantly from 214 to 260° ($F_{(1,230)}$ = 12.76, p < 0.0001). Similarly, preferred firing phase for CA1 place cells in FSE-L shifted significantly from 180 to 235° ($F_{(1,114)}$ = 16.2, p < 0.0001). Preferred firing phase for cells in CA3 remained static between both contexts for both Cont ($F_{(1,74)}$ = 0.009, p = 0.926) and FSE-L ($F_{(1,56)}$ = 2.13, p = 0.150). Moreover, the preferred CA3 phase of firing during task performance was similar for both groups (W–W, $F_{(1,117)}$ = 3.77, p = 0.055). The constant phase preference in CA3 observed in both groups also suggests that phase shifts in CA1 were not due to movement or spatial sampling differences during performance of the active avoidance task. We therefore show that performance of the active avoidance task results in a significant shift in the preferred firing phase of CA1 place cells to a later phase of theta. An example of the shift in preferred phase of firing of a CA1 place cell between foraging and avoidance is shown in Fig. 5 (A–D).

In direct contrast to these groups, CA1 place cells from FSE-NL showed no significant population shifts in the preferred phase of firing between foraging and avoidance tasks (W–W, $F_{(1,98)}$ = 0.147 p = 0.702). Again, this was not a feature of opposing phase preferences in individual animals (Sup. Table 11), as each animal exhibited a phase preference between 178° and 198°. This observation in FSE-NL phase preference constancy is in stark contrast to the uniform shifts toward 270° seen in FSE-L and Cont. In addition, preferred firing phase for FSE-NL cells in CA3 showed a significant change between contexts and fell back from 226°–174° (W–W, $F_{(1,69)}$ = 11.38, p = 0.0012) and thereby showed the opposite trend seen in Cont and FSE-L.

While theta oscillations between CA1 and CA3 are typically out of phase, the robust shift in CA1 phase preference to a later phase of theta, and resulting alignment between the preferred phase of CA1 and CA3 cell firing, suggests that dynamic temporal coordination

between the two structures is a necessary network feature of task performance.

3.5.4. Firing Probability Matches Phase Preference Results

We also examined the probability of cell firing for CA1 and CA3 place cells in 30° bins between 30° and 360° (Fig. 6). The results of this analysis were in agreement with the circular analysis in Fig. 4. The CA1 place cells of Cont and FSE-L tended to shift their preferred phase of firing to the descending phase of theta between foraging and avoidance and were more in register with the static phase preference in CA3. Again, FSE-NL CA1 place cells did not demonstrate a preferred phase of firing within the theta cycle. Correlation values of each of the curves in Fig. 6, comparing firing probability by recording region and context, is shown in Sup. Table 12.

3.6. LFP Voltage Correlations Between CA1 and CA3 Vary by Group

Phase preference analysis implies that shifting CA1 phase preference in a manner that aligns with CA3 phase preference may be necessary to perform the active avoidance task. That FSE-NL did not exhibit this shift could be due to alterations in circuit efficacy within CA1 or between CA1 and CA3 that may ultimately underlie FSE-NL difficulties with the active avoidance task.

We analyzed the linear relationship between speed and CA1 theta frequency (see Sup Figs. 8–9) for animals in each group and found that while there was no difference between Cont and FSE-L, there was a significant difference between Cont and FSE-NL (see supplementary results). Put simply, when animal speed increased, the frequency of CA1 theta in FSE-NL was less likely to also increase in a linear fashion.

We also calculated the normalized LFP voltage correlations between simultaneously recorded probes in CA1 and CA3 for Cont (Fig. 7A), FSE-L (Fig. 7B), and FSE-NL (Fig. 7C) in order to test for group differences in the efficacy of communication between these hippocampal subregions during theta related brain states while exploring the stable arena. We looked at the voltage correlation between the theta band of CA1 and frequencies between 1 and 120 Hz in CA3 (Fig. 7D) and vice versa (Fig. 7E). The results of the voltage correlation analysis examining correlation for each individual group relative to 0 are described in supplementary results. The results of Group x Frequency (GxF) interaction analysis are described below.

3.6.1. CA1 Theta — CA3 Voltage Correlations: GxF Interaction

We conducted GxF analyses for CA1-CA3 and CA3-CA1 voltage correlations to examine putative differences between groups. Significant GxF interactions were found between Cont and both FSE-L (p < 0.001) and FSE-NL (p < 0.001) (see bottom Fig. 7D). With regard to the Cont comparison with FSE-L, the significantly different frequencies between the groups were band specific (see Sup. Table 4). The Cont had significantly greater correlations at the peak of the theta band (8.94 Hz; p = 0.03) and significantly lower correlations toward the low end of slow gamma (22.35–37.25 Hz; p-values indicated in Sup. Table 5) than FSE-NL. The FSE-L also had significantly lower correlations than FSE-NL at frequencies in the slow gamma range (25.33–55.13 Hz; p values indicated in Sup. Table 6).

3.6.2. CA3 Theta — CA1 Correlations: GxF

Significant GxF interactions were found between Cont and FSE-L (p < 0.001) and FSE-NL (p < 0.001) (see bottom Fig. 7E). With regard to the comparison with FSE-L, the correlations again tended to be significantly lower for the FSE-L than both Cont and FSE-NL in the slow gamma range (Sup. Tables 7 and 8). FSE-NL tended to show higher correlations in the delta band and lower correlations in the theta band than Cont (Sup. Table 9).

This comparison between groups indicates a lower theta band correlation between CA1 and CA3 in FSE-NL that is indicative of disrupted

synaptic communication between the two structures. In addition, the results also indicate a lower correlation between theta and gamma in FSE-NL. This may be related to a reliably slower CA1 gamma frequency evident in both recording contexts (see supplementary results). FSE-L gamma slowing and the ability to segregate epochs of theta and gamma between CA1 and CA3 may therefore represent adaptive network mechanisms in this group that allow for task performance.

4. Discussion

In an established model of experimental FSE, we found rats that developed cognitive impairment while others did not (Barry et al., 2015). These observed differences in cognitive outcome in the active avoidance task are paralleled by robust and divergent changes in levels of temporal coordination in place cells recorded from both FSE-L and FSE-NL. Based
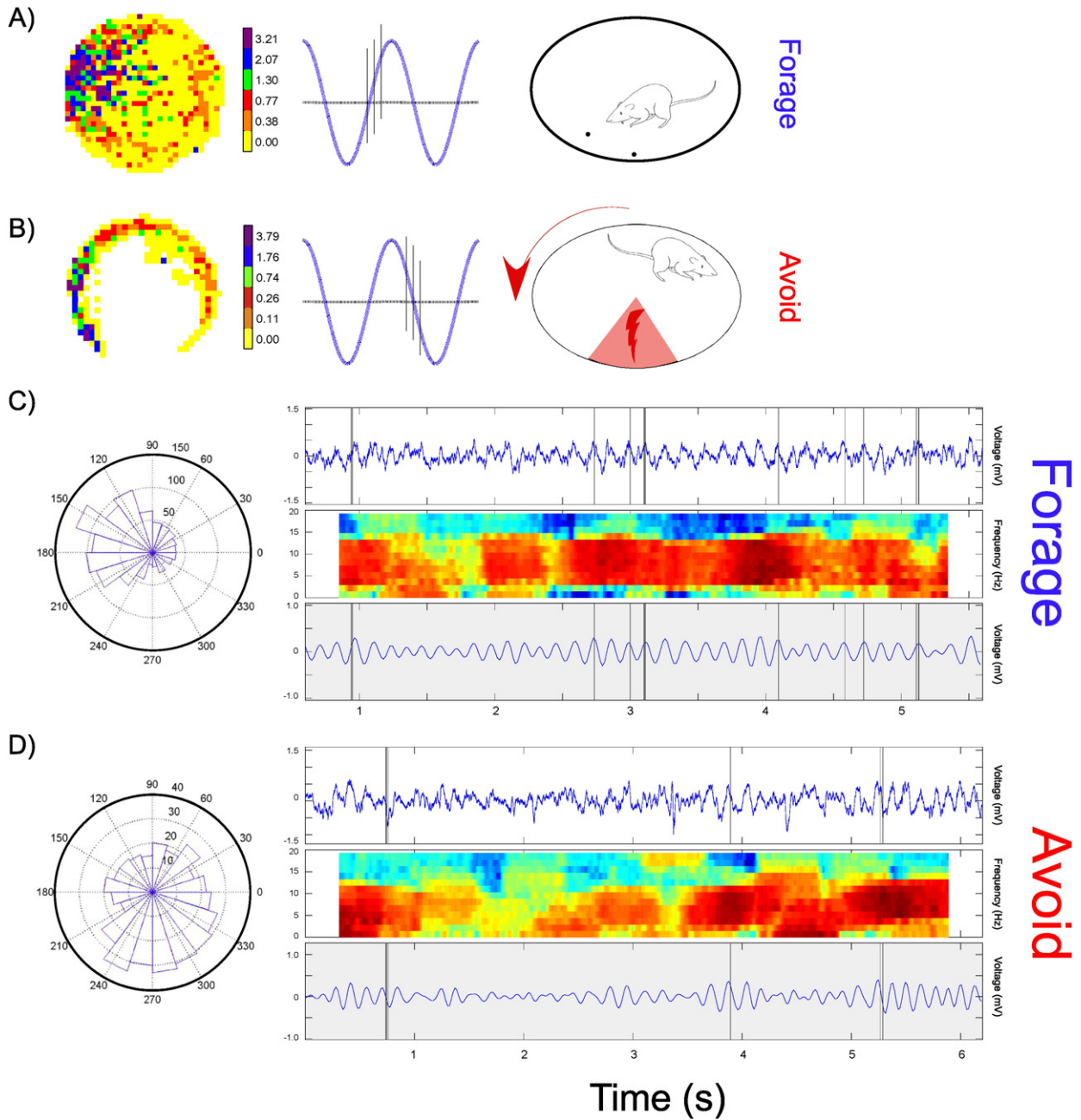

Fig. 5. Illustration of shift in preferred phase of firing of a hippocampal place cell within the local theta cycle between foraging and avoidance contexts. A) Rate map showing a place cell firing field (left) during a foraging session on the stable arena (right) that preferred to fire in the ascending phase of theta (middle); B) Rate map for the same cell in A that also had a place cell firing field (left) during an active avoidance session on the rotating arena (right) that shifted its tendency to fire to the descending phase of theta (middle); C) Roseplot histogram (left) where the number of action potentials for the cell in A are binned by 20 18° bins (0–360°). The spectrogram for a 5-sec period of recording is shown between the raw (top) and filtered (5–12 Hz) EEG signal. Black lines indicate when these action potentials occur within the ascending phase of the raw and filtered EEG traces; D) Roseplot histogram (left) where the number of action potentials for the cell in B are binned by 20 18° bins (0–360°). The spectrogram for a 6 sec period of recording is shown between the raw (top) and filtered (5–12 Hz) EEG signal. Black lines indicate when these action potentials occur within the descending phase of the raw and filtered EEG traces.
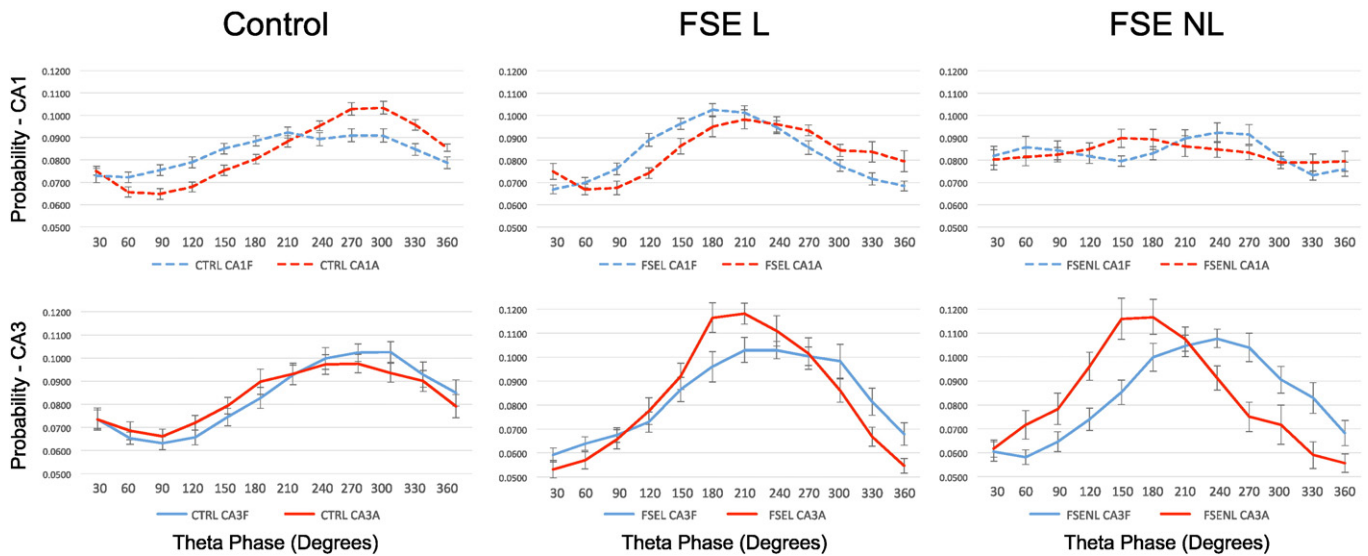
Fig. 6. Average and standard error of firing probability of spatially tuned cells relative to local theta in CA1 (top) and CA3 (bottom) during foraging (blue lines) and avoidance sessions (red lines) for Cont (left), FSE-L (middle), FSE-NL (right) groups. left) CA1 place cells recorded from Cont were distributed throughout the theta cycle during foraging but showed an increased tendency to fire during avoidance (Top Left) that more closely matched the static preferred phase of firing of cells recorded in CA3 (bottom left); Middle) CA1 place cells recorded from FSE-L during foraging showed a greater tendency to fire at the peak of theta in comparison to Cont. As in Cont, the preferred phase of firing shifted to the descending phase of theta during avoidance (top middle) and more closely matched the preferred phase of firing in CA3 (bottom middle); Right) In agreement with Fig. 6, CA1 place cells recorded from FSE-NL during foraging and avoidance did not show a preferred phase of firing within the theta cycle (top right). CA3 place cells also showed an uncharacteristic shift of preferred phase toward the peak of theta (bottom right).

on our key findings, we propose that temporal discoordination observed in FSE-NL ultimately leads to the inability to appropriately organize the routing of spatial information between CA1 and CA3 subregions of the hippocampus. That the FSE-L tendency for baseline place cell phase preference toward the peak of theta indicate that rather than being spared by FSE, their networks were able to adapt in a manner that may have allowed for performance of the active avoidance task. These results are important as they suggest that long-term effects of pediatric seizures impact the temporal organization of hippocampal place cells in a manner that ultimately determines the ability to learn and perform a complex spatial task.

If theta oscillations are the resultant physiological correlate of behavioral navigation and exploration (Buzsaki, 2002) and if hippocampal pyramidal cells generate internal maps to guide the animal's spatial behavior (O'Keefe and Nadel, 1978), then there should be a connection between them. The precision of place cell spike timing within theta carries information relevant to the integration of neural information with its downstream target and for normal cognitive processes (Buzsáki, 1994; Dayan and Abbott, 2001). Phase preference of place cell action potentials (Mizuseki et al., 2009; Schomburg et al., 2014; Douchamps et al., 2013; Siegle and Wilson, 2014) can, in effect, therefore be thought to combine space and time in the service of learning and memory. Our Cont results during the foraging context are in good correspondence with the descriptions of phase preference described previously (Mizuseki et al., 2009), particularly with a preference for CA1 pyramidal cells to fire over a 180° range. Similarly, there was a tendency for CA3 pyramidal cells to cluster in a narrower range of theta, resulting in a larger resulting mean vector length in CA3 than CA1.

The preferred phase of firing of hippocampal cells in CA1 can be altered depending on brain states that underpin the encoding or recall of information in relation to the different plasticity regimes that these modes require during the course of varying synaptic inputs from either CA3 or the entorhinal cortex (Hasselmo, 2005; Siegle and Wilson, 2014). Synaptic conditions in CA1 are believed to be optimal for increased plasticity and the encoding of

information at the peak of the pyramidal layer theta, coinciding with inputs from the entorhinal cortex (Douchamps et al., 2013; Hasselmo, 2005). The direct inputs from entorhinal cortex to CA1 have also been implicated in the spatial specificity of CA1 place cells (Brun et al., 2002). The concept that this pathway has an important role in plasticity largely stems from experimental work that has shown that electrical stimulation at the peak of local theta induces long-term potentiation (LTP) (Holscher et al., 1997; Huerta and Lisman, 1995). Synaptic conditions in CA1 are more optimal for the recall of information at the trough of local theta when synaptic inputs from CA3 are strongest (Hasselmo, 2005). Recent experiments have also used optogenetics to illustrate Hasselmo's theory of the importance of phase with regard to encoding and recall by improving spatial memory performance through stimulation at the peak and trough of theta (Siegle and Wilson, 2014).

The CA1 place cells of FSE-L were more likely to show a more robust phase preference toward the peak of local theta than Cont rats. In accordance with Hasselmo's theory (2005), this feature may represent a compensatory mechanism that altered CA1 temporal dynamics in a manner that could lead to a baseline network state that could promote LTP, enhance the acquisition of information and offset cognitive deficits. A lack of phase preference and increased CA1 temporal discoordination could lead to a baseline network state that is unable to encode task parameters, as was evident for FSE-NL in our experiment. However, while FSE-NL show clear difficulties in spatial processing, they were able to learn and assign valence to each context based on the presence of food reward or aversive shock as previously shown in Moita et al. (2004). Yet, the inaccurate spike timing of place cells within theta oscillations yielded a map that could not organize spatial behavior that would allow for accurate clearance of the shock zone. This notion is discussed in more detail below.

Changes in preferred firing phase have previously been described with regard to exposure to novelty (Douchamps et al., 2013) as well as between the center and side arms of a spatial alternation task (Schomburg et al., 2014). Our results show that phase modulation of cell activity, as well as robust phase shifts in response to cognitive
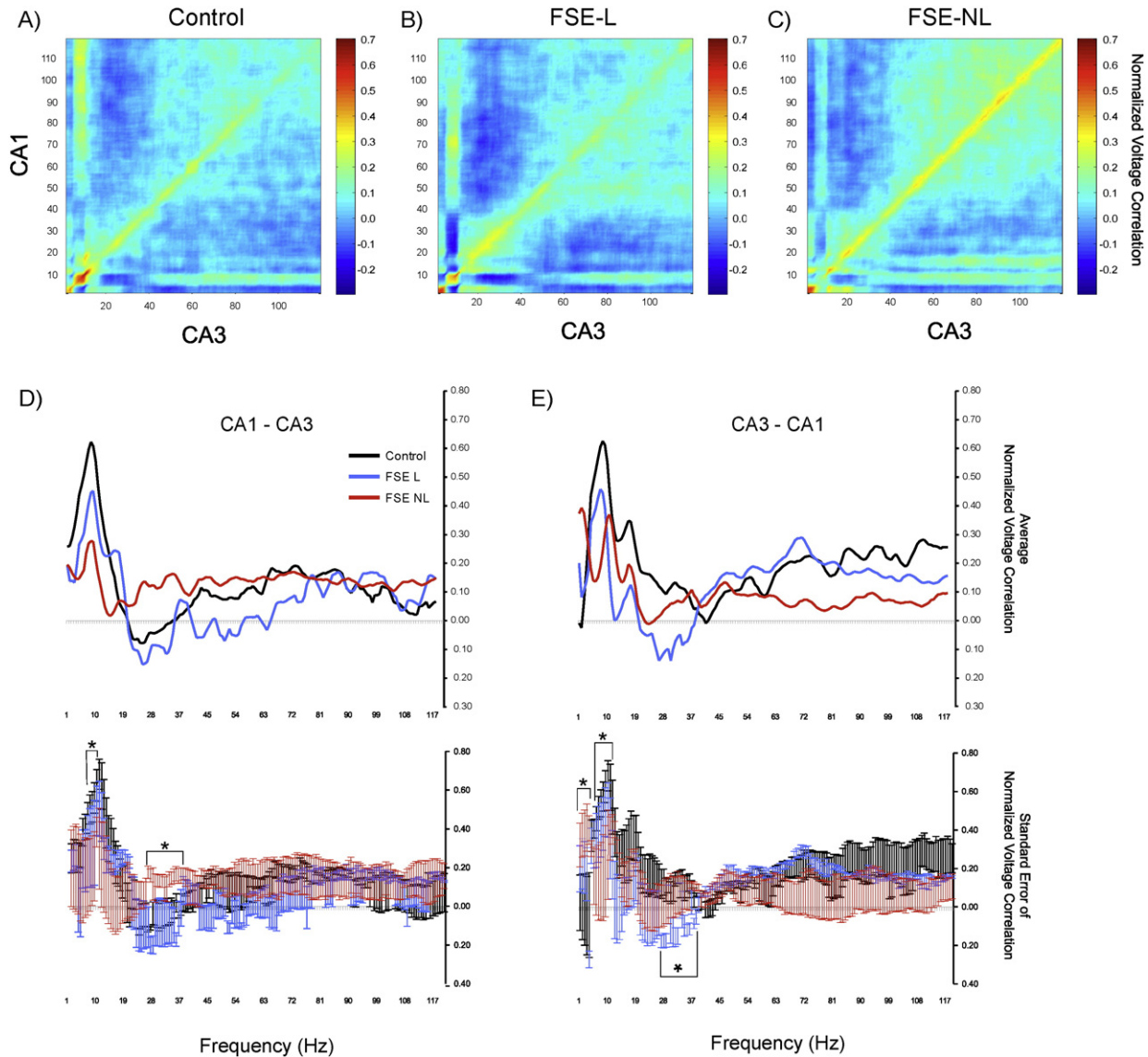
Fig. 7. Cross correlograms showing voltage correlations between simultaneously recorded probes in CA1 and CA3 during foraging for Cont (A), FSE-L (B) and FSE-NL (C). D) Top: Moving average of voltage correlations for CA1 theta bands compared to 0–120 Hz in CA3 for Cont (black line), FSE-L (blue line) and FSE-NL (red line); Bottom: Standard error for each group and frequency. Asterisks indicate bands of significant group by frequency interactions. FSE-NL exhibit lower cross theta correlations and higher slow gamma correlations than Cont. FSE-L and Cont are generally similar. E) Top: Moving average of voltage correlations for CA3 theta bands compared to 0–120 Hz in CA1 for each group; Bottom: Standard error for each group and frequency. FSE-NL exhibit higher delta correlations and lower cross theta correlations than Cont. While generally similar to Cont, FSE-L show decreased slow gamma correlations.

demand, illustrate network adaptation or malfunction as a long-term consequence of pediatric seizures. Remarkably, the shifts in preferred phase preference between foraging and avoidance contexts, for both Cont and FSE-L brought the preferred firing phases of place cells in both CA1 and CA3 in register at a specific phase of theta. That CA3 phase preference was static in both groups and in both contexts suggests that the shift in phase preference in CA1 during active avoidance was not due to changes in spatial sampling. As this shift was not seen in FSE-NL, this implies that performance in the active avoidance task may not only be dependent on the temporal organization of action potentials within local theta but that this temporal organization must be aligned between CA1 and CA3 at the descending phase of local theta. Again, these results are very much in line with the notion that the recall of information requires the interaction of CA1 with stored information in CA3 (Hasselmo, 2005).

Theta oscillations are strongly tied to processes in the hippocampus that integrate past and current position with projected position (Gupta

et al., 2012; Itskov et al., 2008). The representation of space by theta-time-scale is similar for CA3-CA1 neuron pairs, yet the firing probabilities of CA1 and CA3 cells are different in the baseline foraging context. CA1 cells tend to fire toward the peak of local theta while CA3 cells are more active toward the trough. This anti-phase relationship is believed to be due to the functional connections within the CA3-CA1 circuit and the unique population dynamics of each region. Temporally coherent increases in gamma power in both regions occur while CA1 and CA3 pyramidal cell layer theta are at opposing levels of excitation (Buzsáki, 2006). This could explain the antithetical relationship we found between CA1 theta and CA3 slow gamma voltage correlations in Cont and FSE-L. In particular, the correlation between CA3 theta and CA1 slow gamma was even lower for FSE-L than Cont and may be related to the slower gamma frequency found in these animals.

FSE-NL exhibited what may be considered a pathologically low cross-theta correlation between CA1 and CA3. Coupled with the observation that CA1 pyramidal cells exhibit temporal discoordination in CA1 with regard to hippocampal theta, our results suggest that a

cause of FSE-NL difficulties with the active avoidance task is ineffective circuit coordination at CA1 synapses that are believed to actively regulate inputs from both CA3 at stratum radiatum and entorhinal cortex at straum lacunosum. The optimal interval between CA3 and entorhinal inputs for discharging CA1 pyramidal cells is 40–60 ms, or half a theta cycle. The major implication here is that an active subset of CA3 cells can "predict" the animal's spatial location 40–60 ms earlier. If the entorhinal input then "confirms" this prediction of spatial location, the CA1 pyramidal cells will become active. If not, the entorhinal input is insufficient to activate CA1 cells (Buzsáki, 2006). Therefore, to calculate current and projected position it is necessary for spike timing to be temporally accurate and for CA3 and CA1 to operate as a functional unit relative to entorhinal cortex inputs during theta. This functional connectivity between CA1 and CA3 is evident in the significant voltage correlations at theta frequency between CA1 and CA3 in animals that are able to learn the avoidance task. Because cross-theta correlations are low in FSE-NL, and CA1 cell activity is not temporally coordinated by theta in these animals, integration of CA1 action potentials with CA3 and entorhinal inputs would be impeded.

We contend that temporal discoordination at CA1 synapses ultimately lead to inaccuracy of position calculation. This calculation would be particularly prone to error during active avoidance when the animal has to regularly update its position relative to the shock zone on a continuously rotating platform. This could explain the inefficient strategies exhibited by FSE-NL, such as simply moving to the center of the arena rather than away from the shock zone. That CA1 cells in FSE-L are more likely to fire at the peak of theta than Cont, coinciding with entorhinal inputs to CA1, and also exhibit alterations in theta/gamma correlation between CA3 and CA1, strongly suggests that there are alterations to the microcircuitry underpinning temporal coordination at CA1 synapses. While the hippocampal network is altered in these animals in comparison to controls, the network is still capable of organizing active avoidance behavior, albeit using a strategy that differs markedly from Cont.

While most children with FSE do well (Verity et al., 1993; Shinnar et al., 2001), our findings in a rat model that mimics the clinical condition (Dube et al., 2006) raises the question of whether children who seemingly do well after febrile status epilepticus actually are spared injury or whether they compensate for the injury. To address this question clinically it will be necessary to do detailed neuropsychological and educational evaluations in children with FSE to determine if they learn differently from children without a history of seizures. If a different learning strategy is detected, learning how children compensate for the injury will be important in developing educational strategies for children with cognitive dysfunction following FSE. Neuronal oscillations, and presumably temporal coding, are malleable with over-training in rats (Kleen et al., 2011) and it is hoped that educational intervention in children would improve temporal coordination.

While improving the temporal coordination of hippocampal neurons in children is one way of attenuating cognitive deficits, an ideal treatment would be stop the cascade of events following FSE that result in these deficits. Our previous work has implied that the metabolic state of the whole brain, as well as the hippocampus and amygdala, in a 2-hour period post FSE can predict cognitive outcome in the active avoidance task (Barry et al., 2015). Therefore, it would be most interesting to see if improving metabolic regulation in the period following FSE would ultimately decrease the likelihood of learning and memory deficits and result in hippocampal networks with normal levels of temporal coordination.

Our results suggest that the mechanism of cognitive dysfunction in adult animals that have had prolonged febrile seizures is the temporal discoordination of place cells in CA1. As these results are correlational, future studies will need to be carried out to find a causal link between the organization of spike timing by theta and cognition as

well as the physiological mechanisms that underpin adjustments to levels of temporal coordination in relation to cognitive outcome post FSE. One way of accomplishing this causal physiological link would be to use optogenetic stimulation of hippocampal place cells to interfere with their temporal coordination within theta oscillations. If our theory is correct, this should lead to the same phenotype that we've observed with FSE-NL and an inability to learn how to avoid the shock zone on the rotating arena.

Animals that were capable of learning the avoidance task exhibited theta phase preference shifts from the peak of theta toward the trough of theta between foraging and avoidance contexts. That this shift coincides with the static preferred firing phase of CA3 implies increased levels of coordination between the hippocampal subfields. Future experiments will determine how and when this shift occurs as a function of the continuum between task-learning and task-memory.

While exceedingly complex, there are several candidate physiological mechanisms that arise as a result of a cascade of events that follow FSE that could ultimately affect temporal coordination over the course of network development. Hyperthermia induced febrile seizures have been found to increase I_h current in hippocampal pyramidal cells, ultimately leading to cellular hyperexcitability (Chen et al., 1999, 2001; Dyhrfjeld-Johnsen et al., 2008). How changes in I_h current, or other FSE induced changes such as inflammatory cascades (Choy et al., 2014) affect the development of the hippocampal microcircuitry that underpins temporal coordination is not yet known. Apart from ion channel alterations, changes to the dendritic structure or number of synapses along the apical dendrites of CA1 cells may be altered following the FSE event. These changes can then dramatically alter the hippocampal network architecture, resulting in either FSE-NL or FSE-NL phenotypes. Alterations of pyramidal cell excitability or interneuron types such as basket cells, oriens-lacunosum moleculare cells (O-LM), or bistratified cells are likely candidates for disrupting temporal organization of the hippocampus. O-LM cells that partner with excitatory inputs from entorhinal cortex at the distal dendrites of CA1 cells while the excitatory input of CA3 cells is matched by the bistratified interneuron family at their inputs to CA1 at stratum radiatum. Finally, the basket family of interneurons fire rhythmic bursts in register with theta oscillations, thereby producing critical inhibitory currents in the region of the pyramidal cell bodies (Klausberger et al., 2003, 2004). More experimental work will be necessary to determine if and how alterations in these cell types following FSE might ultimately affect the microcircuitry of temporal coordination, as determined by the integration of CA1 cell activity with inputs from CA3 or the entorhinal cortex at theta frequency.

We have described cognitive outcome and corresponding physiological changes as discrete conditions, adaptation and dysfunction. We took this tack primarily because the behavioral data we describe here and in our previous work (Barry et al., 2015) strongly indicated a bimodal outcome. FSE rats learn in a similar manner to controls (FSE-L) or they do not learn the task at all, even with generous amounts of extra training (FSE-NL). We credit the nature of the task for pointing to the physiological differences in FSE-L and FSE-NL animals that also appear to be bimodal, with either increased or decreased organization of CA1 place cell activity by theta. It is possible that another spatial task with a larger sample size may be able to find a continuum between alterations in physiology or levels of temporal coordination and performance.

An important implication of our results is that they point to the correct 'scale' of analysis that addresses the possibility of adaptation in FSE-L and malfunction in FSE-NL. The results best represent the 'meso-scale' level of analysis between physiological alterations due to FSE and observable differences in cognitive outcome at the behavioral level. We have shown that the temporal organization of neural discharge within local theta oscillations is altered post-FSE in a manner that reflects an adaptive shift in FSE-L and maladaptive discoordination in FSE-NL. Our findings are therefore in line with the converging notion in the

Appendix A. Supplementary data

Supplementary data to this article can be found online at http://dx.doi.org/10.1016/j.ebiom.2016.03.039.

References

Barry, J., Muller, R., 2011. Updating the hippocampal representation of space: place cell firing fields are controlled by a novel spatial stimulus. Hippocampus 21, 481–494.
Barry, J.M., Rivard, B., Fox, S.E., Fenton, A.A., Sacktor, T.C., Muller, R.U., 2012. Inhibition of protein kinase Mzeta disrupts the stable spatial discharge of hippocampal place cells in a familiar environment. J. Neurosci. 32, 13753–13762.
Barry, J.M., Choy, M., Dube, C., Robbins, A., Obenaus, A., Lenck-Santini, P.P., Scott, R.C., Baram, T.Z., Holmes, G.L., 2015. T2 relaxation time post febrile status epilepticus predicts cognitive outcome. Exp. Neurol. 269, 242–252.
Bender, R.A., Dube, C., Gonzalez-Vega, R., Mina, E.W., Baram, T.Z., 2003. Mossy fiber plasticity and enhanced hippocampal excitability, without hippocampal cell loss or altered neurogenesis, in an animal model of prolonged febrile seizures. Hippocampus 13, 399–412.
Berens, P., 2009. CircStat: a MATLAB toolbox for circular statistics. J. Stat. Softw. 31, 1–21.
Brun, V.H., Otnass, M.K., Molden, S., Steffenach, H.A., Witter, M.P., Moser, M.B., Moser, E.I., 2002. Place cells and place recognition maintained by direct entorhinal–hippocampal circuitry. Science 296, 2243–2246.
Buzsáki, G., 1994. Temporal Coding in the Brain. Springer-Verlag, Berlin; New York.
Buzsaki, G., 2002. Theta oscillations in the hippocampus. Neuron 33, 325–340.
Buzsáki, G., 2006. Rhythms of the Brain. Oxford University Press, Oxford; New York.
Chen, K., Baram, T.Z., Soltesz, I., 1999. Febrile seizures in the developing brain result in persistent modification of neuronal excitability in limbic circuits. Nat. Med. 5, 888–894.
Chen, K., Aradi, I., Thon, N., Eghbal-Ahmadi, M., Baram, T.Z., Soltesz, I., 2001. Persistently modified h-channels after complex febrile seizures convert the seizure-induced enhancement of inhibition to hyperexcitability. Nat. Med. 7, 331–337.
Choy, M., Dube, C.M., Patterson, K., Barnes, S.R., Maras, P., Blood, A.B., Hasso, A.N., Obenaus, A., Baram, T.Z., 2014. A novel, noninvasive, predictive epilepsy biomarker with clinical potential. J. Neurosci. 34, 8672–8684.
Dayan, P., Abbott, L.F., 2001. Theoretical Neuroscience: Computational and Mathematical Modeling of Neural Systems. Massachusetts Institute of Technology Press, Cambridge, Mass.
De Lange, F.P., Jensen, O., Bauer, M., Toni, I., 2008. Interactions between posterior gamma and frontal alpha/beta oscillations during imagined actions. Front. Hum. Neurosci. 2, 7.
Douchamps, V., Jeewajee, A., Blundell, P., Burgess, N., Lever, C., 2013. Evidence for encoding versus retrieval scheduling in the hippocampus by theta phase and acetylcholine. J. Neurosci. 33, 8689–8704.
Dube, C., Chen, K., Eghbal-Ahmadi, M., Brunson, K., Soltesz, I., Baram, T.Z., 2000. Prolonged febrile seizures in the immature rat model enhance hippocampal excitability long term. Ann. Neurol. 47, 336–344.
Dube, C., Yu, H., Nalcioglu, O., Baram, T.Z., 2004. Serial MRI after experimental febrile seizures: altered T2 signal without neuronal death. Ann. Neurol. 56, 709–714.
Dube, C., Richichi, C., Bender, R.A., Chung, G., Litt, B., Baram, T.Z., 2006. Temporal lobe epilepsy after experimental prolonged febrile seizures: prospective analysis. Brain 129, 911–922.
Dube, C.M., Zhou, J.L., Hamamura, M., Zhao, Q., Ring, A., Abrahams, J., Mcintyre, K., Nalcioglu, O., Shatskih, T., Baram, T.Z., Holmes, G.L., 2009. Cognitive dysfunction after experimental febrile seizures. Exp. Neurol. 215, 167–177.
Dube, C.M., Ravizza, T., Hamamura, M., Zha, Q., Keebaugh, A., Fok, K., Andres, A.L., Nalcioglu, O., Obenaus, A., Vezzani, A., Baram, T.Z., 2010. Epileptogenesis provoked by prolonged experimental febrile seizures: mechanisms and biomarkers. J. Neurosci. 30, 7484–7494.
Dyhrfjeld-Johnsen, J., Morgan, R.J., Foldy, C., Soltesz, I., 2008. Upregulated H-current in hyperexcitable CA1 dendrites after febrile seizures. Front. Cell. Neurosci. 2, 2.

Fenton, A.A., 2015. Excitation–inhibition discoordination in rodent models of mental disorders. Biol. Psychiatry 77, 1079–1088.
Fisher, N.I., 1993. Statistical Analysis of Circular Data. Cambridge University Press, Cambridge England; New York, NY, USA.
Fox, S.E., Ranck Jr., J.B., 1981. Electrophysiological characteristics of hippocampal complex-spike cells and theta cells. Exp. Brain Res. 41, 399–410.
Gupta, A.S., Van Der Meer, M.A., Touretzky, D.S., Redish, A.D., 2012. Segmentation of spatial experience by hippocampal theta sequences. Nat. Neurosci. 15, 1032–1039.
Harris, K.D., Henze, D.A., Hirase, H., Leinekugel, X., Dragoi, G., Czurko, A., Buzsaki, G., 2002. Spike train dynamics predicts theta-related phase precession in hippocampal pyramidal cells. Nature 417, 738–741.
Hasselmo, M.E., 2005. What is the function of hippocampal theta rhythm?–Linking behavioral data to phasic properties of field potential and unit recording data. Hippocampus 15, 936–949.
Holscher, C., Anwyl, R., Rowan, M.J., 1997. Stimulation on the positive phase of hippocampal theta rhythm induces long-term potentiation that can Be depotentiated by stimulation on the negative phase in area CA1 in vivo. J. Neurosci. 17, 6470–6477.
Huerta, P.T., Lisman, J.E., 1995. Bidirectional synaptic plasticity induced by a single burst during cholinergic theta oscillation in CA1 in vitro. Neuron 15, 1053–1063.
Insel, T.R., 2010. Rethinking schizophrenia. Nature 468, 187–193.
Itskov, V., Pastalkova, E., Mizuseki, K., Buzsaki, G., Harris, K.D., 2008. Theta-mediated dynamics of spatial information in hippocampus. J. Neurosci. 28, 5959–5964.
Jenks, K.R., Lucas, M.M., Duffy, B.A., Robbins, A.A., Gimi, B., Barry, J.M., Scott, R.C., 2013. Enrichment and training improve cognition in rats with cortical malformations. PLoS One 8, e84492.
Klausberger, T., Magill, P.J., Marton, L.F., Roberts, J.D., Cobden, P.M., Buzsaki, G., Somogyi, P., 2003. Brain-state- and cell-type-specific firing of hippocampal interneurons in vivo. Nature 421, 844–848.
Klausberger, T., Marton, L.F., Baude, A., Roberts, J.D., Magill, P.J., Somogyi, P., 2004. Spike timing of dendrite-targeting bistratified cells during hippocampal network oscillations in vivo. Nat. Neurosci. 7, 41–47.
Kleen, J.K., Wu, E.X., Holmes, G.L., Scott, R.C., Lenck-Santini, P.P., 2011. Enhanced oscillatory activity in the hippocampal-prefrontal network is related to short-term memory function after early-life seizures. J. Neurosci. 31, 15397–15406.
Kravljanac, R., Djuric, M., Jankovic, B., Pekmezovic, T., 2015. Etiology, clinical course and response to the treatment of status epilepticus in children: a 16-year single-center experience based on 602 episodes of status epilepticus. Eur. J. Paediatr. Neurol.
Lubenov, E.V., Siapas, A.G., 2009. Hippocampal theta oscillations are travelling waves. Nature 459, 534–539.
Markus, E.J., Qin, Y.L., Leonard, B., Skaggs, W.E., Mcnaughton, B.L., Barnes, C.A., 1995. Interactions between location and task affect the spatial and directional firing of hippocampal neurons. J. Neurosci. 15, 7079–7094.
Martinos, M.M., Yoong, M., Patil, S., Chin, R.F., Neville, B.G., Scott, R.C., De Haan, M., 2012. Recognition memory is impaired in children after prolonged febrile seizures. Brain 135, 3153–3164.
Mazaheri, A., Coffey-Corina, S., Mangun, G.R., Bekker, E.M., Berry, A.S., Corbett, B.A., 2010. Functional disconnection of frontal cortex and visual cortex in attention-deficit/hyperactivity disorder. Biol. Psychiatry 67, 617–623.
Mitra, P., Bokil, H., 2008. Observed Brain Dynamics. Oxford University Press, Oxford; New York.
Mizuseki, K., Sirota, A., Pastalkova, E., Buzsaki, G., 2009. Theta oscillations provide temporal windows for local circuit computation in the entorhinal-hippocampal loop. Neuron 64, 267–280.
Moita, M.A., Rosis, S., Zhou, Y., Ledoux, J.E., Blair, H.T., 2004. Putting fear in its place: remapping of hippocampal place cells during fear conditioning. J. Neurosci. 24, 7015–7023.
Muller, R.U., Kubie, J.L., 1987. The effects of changes in the environment on the spatial firing of hippocampal complex-spike cells. J. Neurosci. 7, 1951–1968.
Muller, R.U., Kubie, J.L., Ranck Jr., J.B., 1987. Spatial firing patterns of hippocampal complex-spike cells in a fixed environment. J. Neurosci. 7, 1935–1950.
Munk, M.H., Roelfsema, P.R., Konig, P., Engel, A.K., Singer, W., 1996. Role of reticular activation in the modulation of intracortical synchronization. Science 272, 271–274.
O'Keefe, J., Nadel, L., 1978. The Hippocampus as a Cognitive Map. Clarendon Press; Oxford University Press, Oxford New York.
Pastalkova, E., Serrano, P., Pinkhasova, D., Wallace, E., Fenton, A.A., Sacktor, T.C., 2006. Storage of spatial information by the maintenance mechanism of LTP. Science 313, 1141–1144.
Richard, G.R., Titiz, A., Tyler, A., Holmes, G.L., Scott, R.C., Lenck-Santini, P.P., 2013. Speed modulation of hippocampal theta frequency correlates with spatial memory performance. Hippocampus 23, 1269–1279.
Robbe, D., Buzsaki, G., 2009. Alteration of theta timescale dynamics of hippocampal place cells by a cannabinoid is associated with memory impairment. J. Neurosci. 29, 12597–12605.
Robbins, A.A., Fox, S.E., Holmes, G.L., Scott, R.C., Barry, J.M., 2013. Short duration waveforms recorded extracellularly from freely moving rats are representative of axonal activity. Front. Neural Circ. 7, 181.
Roy, H., Lippe, S., Lussier, F., Sauerwein, H.C., Lortie, A., Lacroix, J., Lassonde, M., 2011. Developmental outcome after a single episode of status epilepticus. Epilepsy Behav. 21, 430–436.
Schomburg, E.W., Fernandez-Ruiz, A., Mizuseki, K., Berenyi, A., Anastassiou, C.A., Koch, C., Buzsaki, G., 2014. Theta phase segregation of input-specific gamma patterns in entorhinal-hippocampal networks. Neuron 84, 470–485.

Siegle, J.H., Wilson, M.A., 2014. Enhancement of encoding and retrieval functions through theta phase-specific manipulation of hippocampus. Elife 3, e03061.

Shinnar, S., Pellock, J.M., Berg, A.T., O'Dell, C., Driscoll, S.M., Maytal, J., Moshe, S.L., DeLorenzo, R.J., 2001. Short-term outcomes of children with febrile status epilepticus. Epilepsia 42, 47–53.

Toth, Z., Yan, X.X., Haftoglou, S., Ribak, C.E., Baram, T.Z., 1998. Seizure-induced neuronal injury: vulnerability to febrile seizures in an immature rat model. J. Neurosci. 18, 4285–4294.

Van Esch, A., Ramlal, I.R., Van Steensel-Moll, H.A., Steyerberg, E.W., Derksen-Lubsen, G., 1996. Outcome after febrile status epilepticus. Dev. Med. Child Neurol. 38, 19–24.

Verity, C.M., Ross, E.M., Golding, J., 1993. Outcome of childhood status epilepticus and lengthy febrile convulsions: findings of national cohort study. BMJ 307, 225–228.

Ziegler, A., Kastner, C., Blettner, M., 1998. The generalised estimating equations: an annotated bibliography. Biom. J. 40, 115–139.